fire

MDPI

Article

Quantifying Fire-Induced Surface Climate Changes in the Savanna and Rainforest Biomes of Brazil

Fernando De Sales [1,*], Zackary Werner [2] and João Gilberto de Souza Ribeiro [3]

[1] Department of Geography, San Diego State University, San Diego, CA 92182, USA
[2] RedCastle Resources, Salt Lake City, UT 84111, USA; zwerner.author@gmail.com
[3] Environmental Engineering Department, Federal University of Rondonia, Ji-Parana 76900, RO, Brazil; joao.gilberto@unir.br
* Correspondence: fdesales@sdsu.edu

Abstract: This study uses a combined research approach based on remote-sensing and numerical modeling to quantify the effects of burned areas on the surface climate in the two Brazilian biomes most affected by fires: the tropical savanna and the Amazon rainforest. Our estimates indicate that between 2007 and 2020, approximately 6% of the savanna and 2% of the rainforest were burned on average. Non-parametric regressions based on 14-year climate model simulations indicate that latent heat flux decreases on average by approximately 0.17 W m^{-2} in the savanna and 0.60 W m^{-2} in the rainforest per each 1 km^2 burned, with most of the impacts registered during the onset of the wet season. Sensible and ground heat fluxes are also impacted but at less intensity. Surface air is also warmer and drier, especially over rainforest burned sites. On average, fire reduced gross primary production in the savanna and rainforest by 12% and 10%, respectively, in our experiments.

Keywords: fire; burned areas; Amazon rainforest; Cerrado; savanna; surface climate; surface heat fluxes

Citation: De Sales, F.; Werner, Z.; de Souza Ribeiro, J.G. Quantifying Fire-Induced Surface Climate Changes in the Savanna and Rainforest Biomes of Brazil. *Fire* **2023**, *6*, 311. https://doi.org/10.3390/fire6080311

Academic Editors: Carlos A. C. dos Santos, Luiz E. O. C. Aragao, Paulo Artaxo, Gabriel de Oliveira, Guilherme A. V. Mataveli, Maquelle Garcia and Hannah Stewart

Received: 24 July 2023
Revised: 9 August 2023
Accepted: 10 August 2023
Published: 12 August 2023

1. Introduction

Fire is a natural phenomenon in the Earth system that has shaped the landscapes and ecosystems of many of Earth's biomes for millennia [1–3]. While its occurrence has been worldwide and inconspicuous throughout the Holocene including the anthropogenic use in land management [4], recent outbreaks in Amazonia [5], western North America [6,7], southern Europe [8], and Australia [9] have underscored the threats that fires pose to human safety, biodiversity, and ecosystem health. These events have also raised concerns about the long- and short-term effects of fires on the global and regional climate [10–14].

Fires impact the global climate primarily through the emission of greenhouse gases and by limiting atmospheric carbon sequestration. It is estimated that fires burn around 4 million km^2 and emit approximately 8 billion tons of CO_2 into the atmosphere on average in a year [15,16]. Furthermore, they influence Earth's climate by limiting gross primary productivity globally by around 10% [17]. On the other hand, fires can affect the climate regionally by altering land surface albedo and roughness, disrupting water and energy budgets [6,11], and through aerosol–cloud interactions that lead to complex climate–fire feedbacks [18].

For example, study [10] suggests that fires may be linked to changes in the Northern Africa monsoonal rainfall due to reduced radiative heating that tends to stabilize the atmosphere. Additionally, [19] concludes that the radiative effect of fire aerosol–cloud interactions generally leads to cooling effects in most regions due to scattering and reflections by enhanced cloudiness, especially in high-latitude regions. While the role of fires on the large-scale climate is more evident, the local consequences to surface and boundary-layer climates are less understood, and often omitted in weather and climate modeling studies and forecasts.

Most northern and central Brazilian biomes are subjected to natural and anthropogenic fires to a certain extent. Savanna, grasslands, shrubland, and the rainforest are all burned by humans for different purposes and land uses, though the natural potentials for burning are very different among vegetation types [20]. Anthropogenic fires are frequent in both the fire-adapted savanna (regionally known as Cerrado) and the fire-sensitive rainforest of northern and central Brazil.

In addition to being a biodiversity hotspot, the Amazon rainforest provides a wealth of ecosystem services of recognized global importance, including the regulation of global temperature and precipitation regimes and agricultural production. Mostly located in a humid tropical ecoregion, the rainforest is naturally more resistant to the occurrence of large fires [20]. However, when fires do occur, they result in substantial ground cover removal and tree loss with significant impacts to momentum, energy, and water fluxes at the surface. This deforestation process has serious regional environmental consequences and contributes globally to climate change, since the Amazon plays an important role in carbon storage, which is released into the atmosphere during fires [21]. Deforestation acceleration in the region has been linked to monoculture expansion in pasture areas, which results in livestock displacement to forested areas, and to the recent weakening of environmental agencies and legislation [22].

The Brazilian Cerrado is the second largest biome in South America and the most biodiverse savanna in the world. With an area approximately half of that of the Amazon rainforest, it concentrates 5% of the planet's species and is home to 40% of Brazil's water production. Unlike the rainforest, the Cerrado savanna is an adapted and fire-dependent ecosystem [20]. In this ecoregion, trees have developed fire protection mechanisms, such as thick barks, that protect the heartwood of trees [23].

This study aims to quantify the impacts of large fire activity in the Brazilian savanna and rainforest biomes, using the latest in modeling and remotely-sensed land and vegetation conditions. The objective is to contribute to the scientific understanding of the effects of fire-induced vegetation and soil degradation on the surface energy balance and heat fluxes responsible for driving the hydrologic and warming cycles, boundary layer evolution, and maintaining photosynthetic activity. The study relies on state-of-the-art land-surface model simulations driven by satellite-derived burned area and vegetation information, and meteorological conditions obtained from atmospheric reanalysis.

2. Data and Methods

2.1. Burned Area Fraction

The Moderate Resolution Imaging Spectroradiometer (MODIS) approximate date-of-burning product MCD64A1 was used to determine the burned area fraction (BAF). Burned areas are characterized by deposits of ash and charred material, the removal of vegetation, and alteration of the vegetation structure [24]. The product mapping algorithm takes advantage of these temporal and spectral changes to detect the approximate date of burning at a spatial resolution of 500 m by locating the occurrence of rapid changes in daily surface reflectance [25]. It should be noted that, due to its relatively coarse resolution, MCD64A1 omits small burns compared to more recent products. Therefore, our results apply only to fires large enough to be captured by the MODIS sensor.

The methodology to obtain daily BAF from approximate date-of-burning maps has been described in work by De Sales et al. [10]. In summary, the monthly unburned–burned binary masks are initially obtained from the MCD64A1 product, which are then aggregated onto the same grid used for the model simulations using a grid-cell averaging method. The resulting monthly BAF maps are, thus, consistent with the grid resolution and with the vegetation cover representation in the model. Subsequently, daily burned area fractions are calculated for each domain grid cell using a simple linear interpolation.

This approach has been used in other studies [6,11], and it was chosen to minimize the effects of missing information from those periods when the satellite retrieval algorithm could not find enough data to determine ground reflectance, as well as the periods of sensor

malfunctions and cloud contamination. BAF was calculated for the period between January 2007 and December 2020 for the entire country of Brazil, but only information contained within the study area, indicated in Figure 1a, was used in the study.

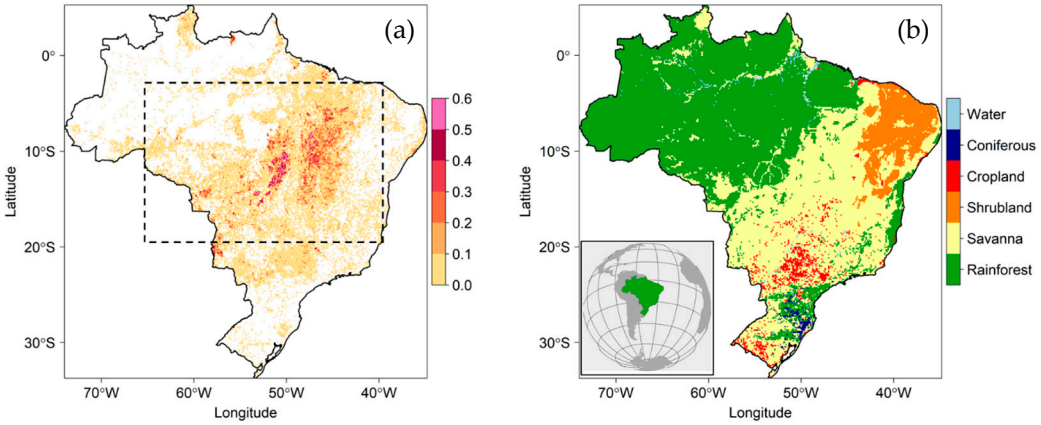

Figure 1. (**a**) 2007–2020 average burned area fraction and (**b**) land cover types (biomes) in Brazil aggregated to the model (7.5 × 7.5 km) grid. The rectangle in (**a**) represents the study area and the domain extent for the model simulations.

2.2. Study Area

Fires were widespread in northern and central Brazil between 2007 and 2020 (Figure 1a). Most parts of the country experienced some fires during those years, except the extreme south and northwest regions. Areas located between 20° S and 5° S, and 65° W and 40° W were particularly affected by fires, with large extents of them experiencing a BAF of over 10%. Hereafter, the area delimited by these four coordinate points is referred to as the study area, which also represents the extent of the model simulation domain. The land cover distribution within the study area is restricted to rainforest in the north and west flanked by sprawling tropical savanna to the east and south, and semiarid shrublands to the far east. Croplands are sparse and scattered primarily in the southern portion of the area. Savanna occupies approximately 50.6% of it, while rainforests, shrublands, and croplands each cover about 41.5%, 6.8%, and 1.1% of the area, respectively (Table 1).

Table 1. The 2007–2020 average vegetated cover fraction, annual burned area, annual fraction burned, and survival rate for the three major land cover types in the study area. "Others" includes shrublands and croplands.

Biome	Vegetated Cover Fraction (%)	Annual Burned Area (10^3 km^2)	Fraction of Land Cover Burned (%)	Survival Rate (%)
Savanna	50.6	116.0 ± 59.5	5.7 ± 2.9	15
Rainforest	41.5	34.2 ± 22.2	2.0 ± 1.3	75
Others	7.9	3.7 ± 1.9	1.1 ± 0.6	0.0

Studies have shown that tropical rainforests, such as the Amazon, cannot tolerate burning, and after a few repeated fires, changes in structure and composition may result in shifts to either a degraded rainforest or a savanna-like environment [26,27]. Currently, the rainforest is the main biome in northern and northwestern Brazil (Figure 1b). On the other hand, open savannas and grasslands, located in central Brazil, are fire-adapted and fire-dependent ecosystems (Figure 1b). With longer and warmer dry seasons, savanna biomes become very flammable and fire outbreaks naturally caused by lightning are also common at the beginning of the wet season [28].

Savanna and rainforest are the primary land cover types affected by fires within the study area. Our calculations indicate that, on average, approximately 73% and 22% of the

burned area registered by MODIS between 2007 and 2020 was located in the savanna and rainforest ecoregions, respectively. On average, approximately 116 × 10^3 and 32 × 10^3 km^2 of savanna and rainforest were burned annually during that period. Shrublands and croplands together averaged nearly 3.7 × 10^3 km^2 of the burned area per year.

The extent of burned areas within the study area had a large interannual variability between 2007 and 2020 (Figure 2a). Large expanses of the domain were burned in 2007 and 2010 (>300 × 10^3 km^2), while 2009 experienced the smallest total burned area (<50 × 10^3 km^2) according to the satellite-based product. In terms of the monthly climatology, the fire season is well defined, with most of burned area concentrated between July and October. Fire activity peaks in September when all major land cover types present in the study area register the largest monthly burned area fractions. On the other hand, April experiences the smallest burned area fraction (Figure 2b).

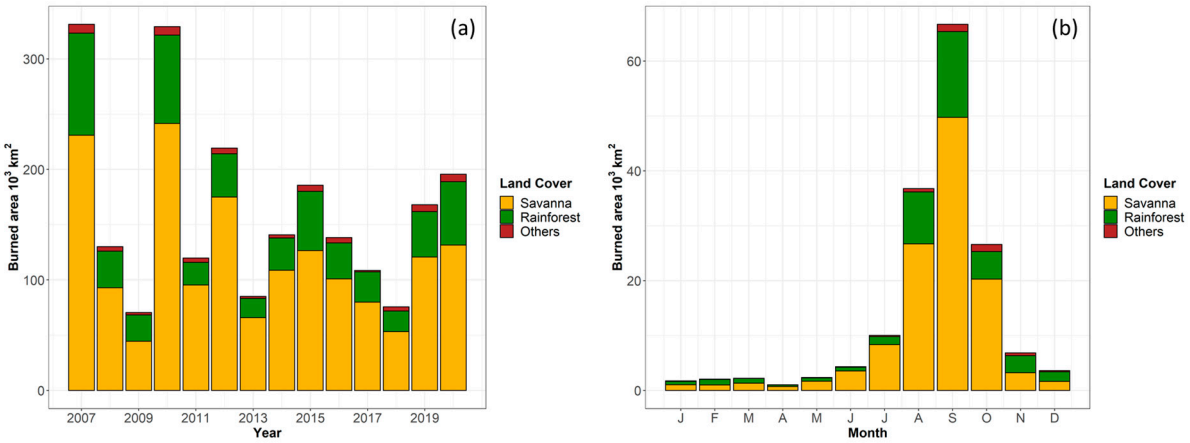

Figure 2. (**a**) 2007–2020 average annual and (**b**) monthly burned area fraction for savanna, rainforest, and minor land cover types located within the study area calculated based on MODIS MCD64A1 product (10^3 km^2). Others includes shrubland, cropland, and grassland land cover types.

2.3. Model and Experiment Design

The objective of this study was to quantify the effects of burned areas on the surface climate of tropical Brazil. To this end, we performed a series of experiments using the second version of the Simplified Simple Biosphere (SSIB-2) land surface model. The SSIB-2 is a biophysical model that calculates photosynthesis-controlled surface processes, while preserving energy, water, and momentum conservation at the atmosphere–land interface [29].

The simulations were carried out for the period between January 2007 and December 2020 in a standalone configuration uncoupled to the atmosphere. Initial and boundary meteorological conditions, including incoming shortwave and longwave radiation, precipitation, and wind speed, were obtained from the ERA5 hourly data set [30]. Vegetation boundary conditions, including the leaf area index (LAI) and vegetation cover fraction (VCF) were prescribed based on MODIS products [31]. The model domain covers approximately 3.5 million km^2 and its spatial resolution was set to 7.5 km to capture the region's land-cover heterogeneity while maintaining the computational feasibility of the simulations (Figure 1a).

Two experiments were conducted. In the first, fire effects were not included and land surface properties were maintained as undisturbed throughout the 14-year model integration. This experiment is referred to the unburned or control. In the second experiment, LAI and VCF were altered based on the burned area fraction described above and on the prescribed fire survival rate of the vegetation type (Table 1). Vegetation cover was updated every 24 h of the simulation following Equation (1), where VCF_u, BAF, and SR represent, respectively, the unburned vegetation cover fraction, burned area fraction, and the vegetation survival rate, which represents the typical vegetation resistance to burning

during a fire. The vegetation fire survival rates used were based on estimates described in [10]. A similar formula was used to alter LAI.

$$VCF = VCF_U(1 - BAF(1 - SR)) \quad (1)$$

In addition to consuming vegetation, one of the most noticeable physical effects of fire on burned surfaces is the deposition of ash. Ash affects the surface energy balance primarily through changes to albedo [32,33]. For the purpose of this study and due to the limited number of observations on post-fire ash albedo for the study area, both shortwave and near-infrared ground albedos were arbitrarily set to 0.01 over the burned fraction of the grid cell to simulate temporary post-fire soil darkening.

2.4. Ash Removal and Vegetation Recovery

Immediately after a fire, a burned area's albedo decreases, then slowly increases as ash and charred materials are removed by wind and rainfall [34]. Similarly, post-fire vegetation often recovers, especially during the following wet season [35,36]. These processes affect heat and water fluxes between the surface and the atmosphere as they drive slow surface-property changes in burned scars [6,37].

Accurate estimates of ash removal and vegetation recovery times are important for simulating the effects of fire on the surface climate correctly; however, obtaining in situ values for these parameters is difficult as vegetation species, fire intensity, and post-fire meteorological conditions vary greatly both spatially and temporally in the study area. Instead, we relied on the MODIS enhanced vegetation index [38] and the surface albedo [39] products to estimate the average vegetation recovery and ash removal times in the study area. Figure 3 exemplifies the methodology used to estimate the ash removal time.

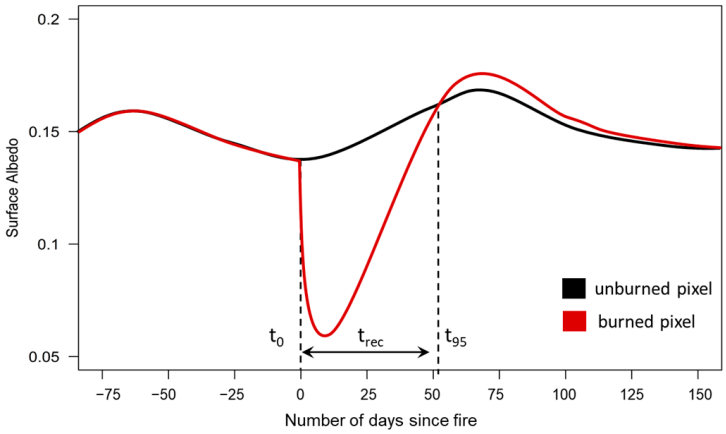

Figure 3. Diagram depicting the methodology used to estimate the post-fire ash removal time (t_{rec}) for surface albedo following a fire. t_0 indicates the fire day and t_{90} represents the day at which a burned-pixel albedo returns to within 95% of its average unburned value.

We started by choosing arbitrary numbers of burned and nearby unburned pixels in the study area. Unburned pixels were considered valid if they exhibited a similar albedo magnitude and variability as the nearby burned pixels over a period of two years prior to the fire. By comparing the burned and unburned shortwave albedo time series, we can determine the day of burning (t_0), as well as a day at which the burned pixel albedo value returns to within 95% of the nearby unburned pixel (t_{95}). The procedure was repeated several times for other unburned–burned pixel pairs between 2009 and 2010, and the average recovery time was then calculated and implemented in the model.

A similar procedure was applied to EVI to estimate the post-fire vegetation recovery average time (Table 2). Our analysis shows that although the biomes have similar ash-removal times, averaging at about 47 days, vegetation recovery varies substantially, with rainforest recovering faster than savanna and other biomes, with an average value

of 173 days for the study area. It should be noted, however, that the vegetation recovery obtained through the EVI analysis does not represent a complete post-fire structural regeneration of the vegetation, but instead it describes solely the time necessary for vegetation to regain its 95% of its radiative properties.

Table 2. Average number of days following fire for 95% of ash removal and vegetation recovery, and the number of pixels used for their estimations for the main biomes and study area average.

Biome	Ash Removal Time (Days)	Vegetation Recovery Time (Days)	Number of Pixels Used in Estimation
Savanna	49	205	15,468
Rainforest	43	132	4255
Others	48	182	4526
Average	47	173	24,249

3. Results

3.1. Model Performance

Before looking at simulated fire impacts, we assessed the SSIB-2 performance by comparing domain-average simulated surface net radiation, sensible heat and latent heat fluxes against NASA Global Land Data Assimilation System (GLDAS) version 2.1 ensemble data. GLDAS is a powerful data reanalysis system built on an uncoupled modeling system that drives multiple land-surface models and integrates a large quantity of observational and satellite-based data in their simulations [40]. Here, we compared data from three GLDAS models, NOAH, VIC, and CLSM, to our simulations. In general, the SSIB-2 radiation variables fell within the GLDAS amplitude range and followed the seasonal cycle correctly (Figure 4a–c). The average root-mean-squared error (RMSE) for surface net radiation, sensible and latent heat fluxes were approximately 8.0, 16.0, 9.0 W m^{-2}, respectively (Table 3). The most noticeable issue with the results was in the summertime sensible heat flux minima, which the model underestimated by approximately 11.0 W m^{-2} on average. Overall, latent heat fluxes were better simulated.

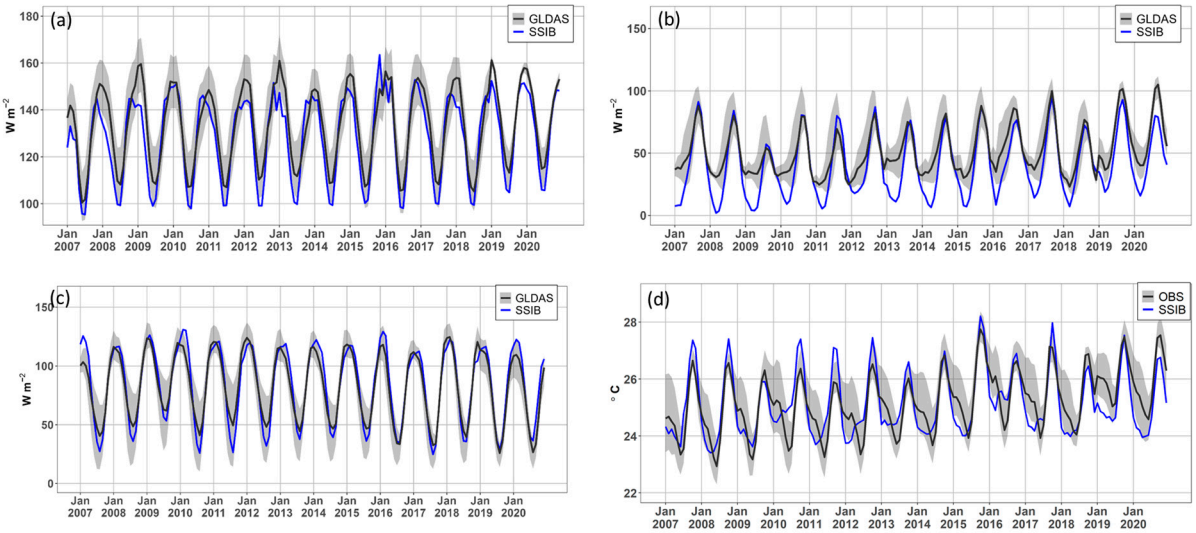

Figure 4. The 2007–2020 domain-average monthly GLDAS ensemble and SSIB-2 surface (**a**) net radiation, (**b**) sensible heat flux, (**c**) latent heat flux, and (**d**) observational analysis and SSIB air temperature. Grey ribbons represent GLDAS and observation maximum and minimum ranges. Benchmark for a, b and c were obtained from GLDAS NOAH, VIC, and CLSM models ensemble analysis, and temperature calculated from Princeton, GHCN, CRU, and CPC data sets.

Table 3. The 2007–2020 analysis monthly mean and standard deviation, simulation mean bias and standard deviation, mean root-mean-squared error (RMSE), and mean temporal correlation coefficient (TCOR) for surface net radiation, sensible and latent heat fluxes, and air temperature based on Figure 4. Radiation in W m^{-2} and temperature in °C. Radiation and air temperature analyses from GLDAS and observations.

Variable	Analysis Mean ± sd	Simulation Bias ± sd	Simulation Mean RMSE	Simulation Mean TCOR
Net radiation	128.3 ± 17.8	5.0 ± 6.5	8.2	0.9
Sensible heat flux	40.6 ± 25.1	−11.4 ± 11.0	15.8	0.9
Latent heat flux	84.0 ± 31.7	1.2 ± 8.9	9.0	0.9
Air temperature	25.1 ± 1.1	−0.1 ± 0.7	0.8	0.8

We also compared the modeled surface air temperature against a multi-observational analysis formed by the University of Delaware [41], Climatic Research Unit [42], Global Historical Climatology Network [43], and Climate Prediction Center Global Unified Temperature [44] data sets (Figure 4d). Similar to the radiation variables, the model simulated the seasonal cycle of surface temperature reasonably well, with results falling within the observed amplitude range for the most part (Table 3). Simulated peak temperatures were overestimated, while the lows were underestimated for some years. A particular shortcoming of the simulations is seen as a sharp drop in air temperature from late spring to midsummer (November–February), which was not registered in the observations. The observational analyses show a slower cooling trend associated with increasing cloud cover and the developing rainy season. The faster-than-observed simulated cooling leads to negative bias and a lower temperature correlation coefficient compared to the radiation variables.

3.2. Burned Area Effects

The effects of fires on the surface radiation of the savanna and rainforest are shown in Figure 5. Grid cells with a BAF lower than 20% were excluded from the analysis to limit the impact of low-confidence results. Surface net radiation increases gradually between May to October, and peaks in September when there is an additional 5.0 and 3.0 W m^{-2} over the savanna and rainforest burned areas on average, respectively (Figure 5a). The increase is associated with decreasing albedos due to the growing extent of ash-covered burned areas in both the savanna and rainforest during the fire season, which also peaks in September.

From November to April, both the savanna and rainforest burned areas see a decrease in net radiation compared to unburned areas. During these months, burned areas' albedos increase slowly as rainfall and wind remove ash and char materials, leaving lighter-colored bare ground exposed in burned areas compared to unburned terrain. A closer look reveals that the soil darkening effect is slightly stronger in the savanna where fires are more widespread, while the soil brightening effect seems slightly stronger for rainforest burned scars, possibly due to the clearing of denser sunlight-blocking vegetation. On average, albedo decreases by approximately 5.0 and 2.5% during the fire season, and increases by about 1.3 and 2.7% in the following three months in the savanna and rainforest biomes, respectively, compared to unburned areas.

Surface latent heat flux (LHF), or evapotranspiration, decreases over burned areas in both biomes, and remains below unburned levels throughout the remainder of the simulation (Figure 5b). The negative effect of fires in the rainforest increases from May and peaks in October at about −17.0 W m^{-2}. However, in the savanna, most of the impacts are seen between October and January, peaking in December at nearly 8.0 W m^{-2}. By and large, the impacts on latent heat flux are stronger in rainforest burned areas. As the fire season wanes, giving way to the wet season in northern and central Brazil, burned vegetation starts to recover and the difference between burned and unburned latent heat flux diminishes in both ecoregions.

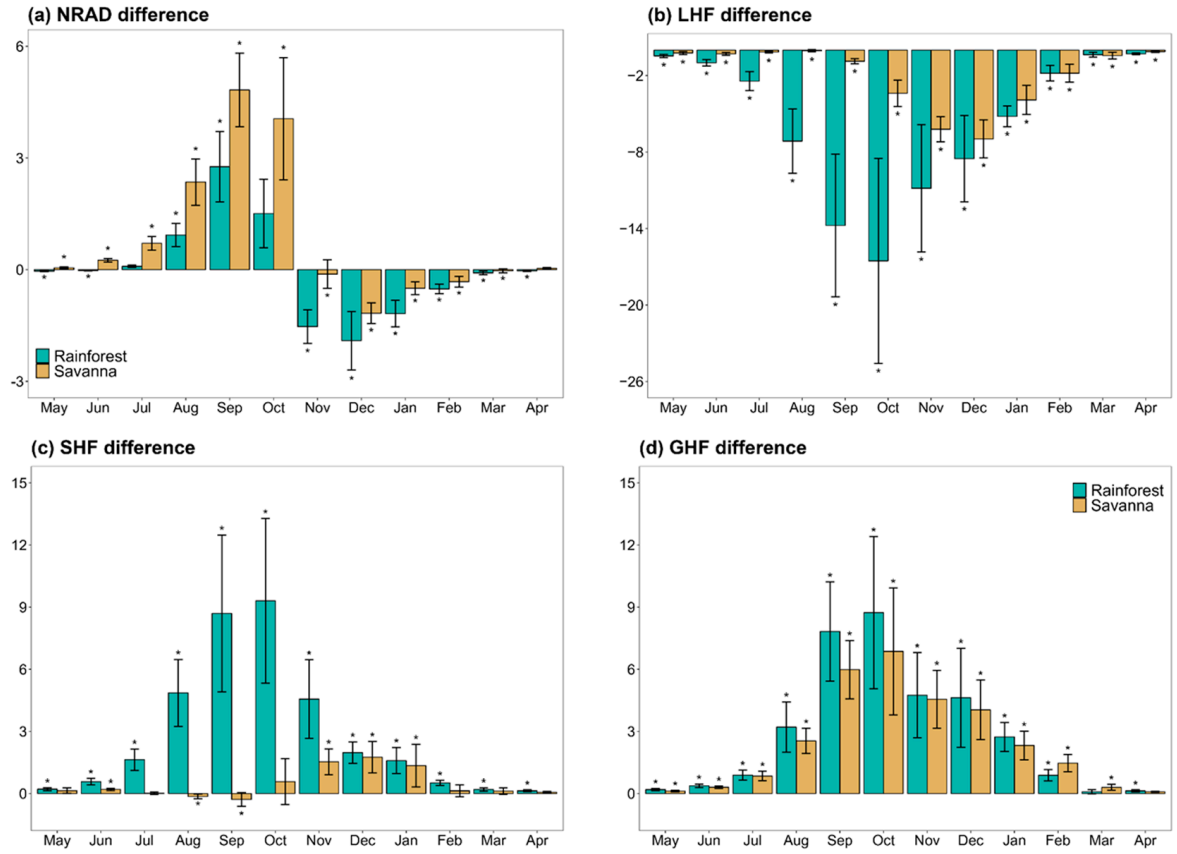

Figure 5. Average monthly difference between burned and unburned (**a**) net radiation, (**b**) latent heat flux, (**c**) sensible heat flux, and (**d**) ground heat flux averaged over savanna and rainforest burned areas (W m^{-2}). Error bars represent one standard deviation from the mean and asterisks indicate the differences that are significant at a 99% confidence level. Only grid cells at least 20% burned are used for this plot.

In general, fires have an opposite effect on sensible heat flux (SHF). Post-fire fluxes over the savanna and rainforest are higher than unburned fluxes on average. Similar to latent heat, however, the impacts start earlier in the rainforest and peak in September and October when burned area fluxes vary between 6.0 and 14.0 W m^{-2} higher than unburned ones. Afterwards, the impacts drop substantially and stay below 5.0 W m^{-2}. The impacts on sensible heat flux are weaker and take place later in savanna burned areas, peaking in December at around 5.0 W m^{-2}. This delay is also observed for latent heat flux (Figure 5a,b).

Ground heat flux (GHF), which represents the daytime loss of energy by heat conduction into the soil, increases in both the rainforest and savanna burned areas. Overall, the changes in the rainforest are similar in magnitude and follow a similar temporal evolution as those for the SHF. On the other hand, savanna GHF changes are nearly twice as large as SHF changes for the same month. We hypothesize that this could be linked to larger fire-induced ground cover removal in the savanna, which allows for the intensification of heat flux into the ground with minimum impacts on sensible heat towards the atmosphere. Overall, our simulations indicate that the variables most impacted by fires are evapotranspiration followed by ground heat flux. Another result is that the fire-season rise in surface net radiation (July to October) does not seem to affect savanna's latent and sensible heat fluxes. This is probably related to the limited availability of surface moisture and vegetation coverage in this ecoregion compared to the wetter and denser rainforest.

The large sample of burn scars of difference sizes in our simulations allows us to establish general relationships between the burned area fraction and changes to the surface climate variables in the savanna and rainforest regions. To calculate these relationships, we employed a non-parametric median-quantile linear regression model [45], which does

not require the usual strict assumption about normally distributed residuals, and is less influenced by extreme outliers in the response variables compared to traditional least-square linear regression estimates that are based on the mean.

In addition to dead plant material, fires consume photosynthetically active vegetation and change soil albedo properties, which ultimately result in post-fire evapotranspiration reduction. Figure 6 describes the LHF response to the burned area fraction in the study area. Evapotranspiration decreases by approximately 0.17 W m^{-2} in the savanna and 0.60 W m^{-2} in the rainforest per each 1 km^2 of burned area (p-value < 0.001). The three-times-larger impact simulated in the rainforest is probably associated with the higher photosynthetic activity rate and water-use efficiency of its vegetation compared to the drier savanna found further south and east.

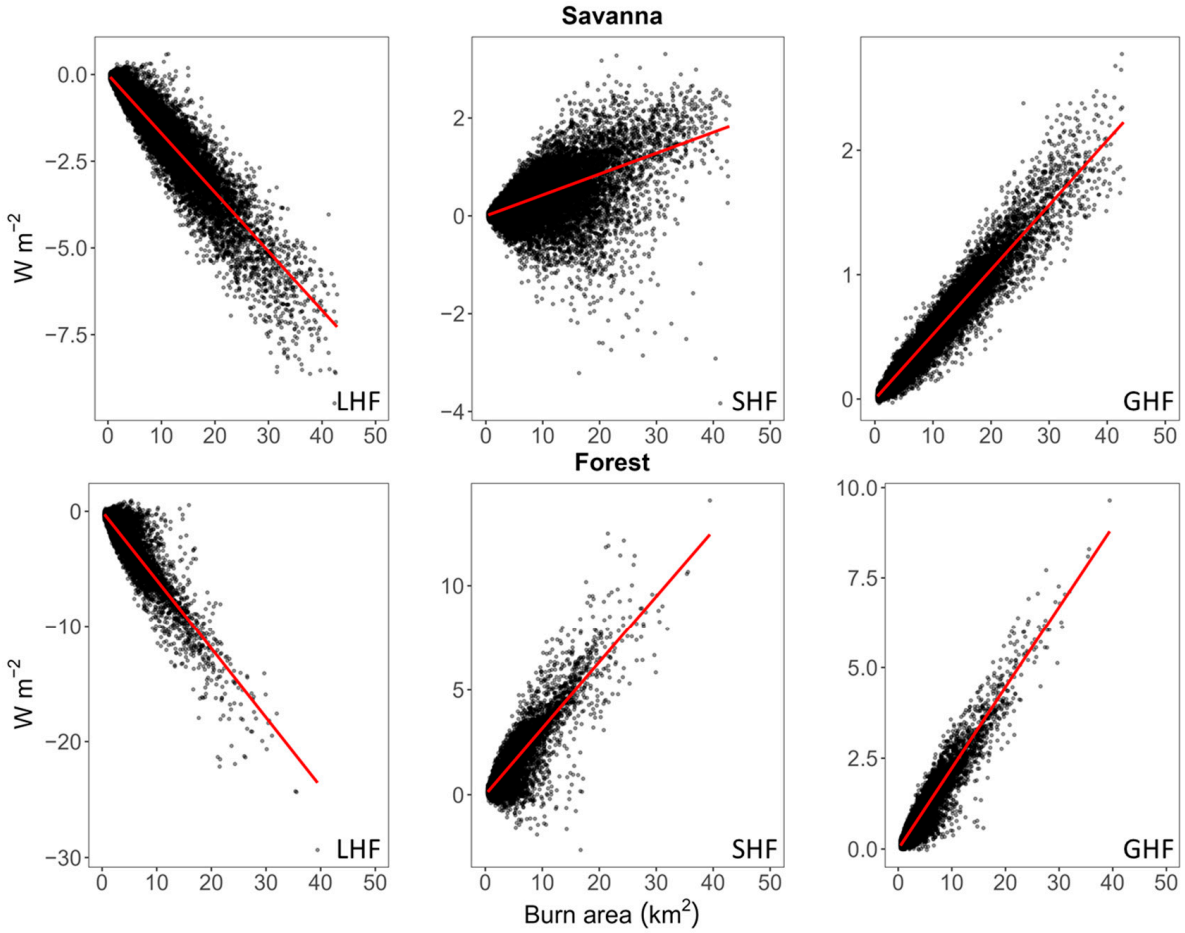

Figure 6. Relationship between latent (LHF), sensible (SHF) and ground (GHF) heat fluxes and burned area fraction for savanna and rainforest burn scars during the fire season (August to November). The red line represents the median quantile regression.

The fire effect on SHF is weaker and more complex (Figure 6). The regression models indicate that SHF increases by 0.04 and 0.32 W m^{-2} per km^2 of burned area in the savanna and rainforest, respectively. However, despite being statistically significant (p-value < 0.001), the linear regression models do not explain the variation in the response data very well, suggesting that there are other important variables when it comes to predicting the effects of fires on sensible heat flux.

This is especially true for the savannas, where small- and mid-size fires cause both an increase and a decrease in sensible heat, while larger burn scars result in increased heat (Figure 6). Since larger fires are often associated with drier weather conditions, perhaps the complex relationship between the burned area and SHF may be linked to the occurrence

of rainfall during or after fires. Further studies are necessary to disentangle the physical processes behind SHF over the burned areas under different post-fire weather conditions.

Unlike sensible heat, fire impacts on GHF are always positive, with 0.05 and 0.22 W m^{-2} per km^2 of the burned area in the savanna and rainforest, respectively (p-value < 0.001). Similar to latent and sensible heat, the changes in ground heat flux per km^2 are greater in the rainforest than in the savanna of northern Brazil. The statistical metrics of the linear regressions in Figure 6 are included in Table 4.

Table 4. Slope (W m^{-2} per km^2 of burn area) and coefficient of determination (pseudo R^2) of the median-quantile linear regressions in Figure 6. All the regressions have p-values lower than 0.001. Pseudo R^2 is described in [45].

Flux	Regression Slope		Pseudo R^2	
	Savanna	Rainforest	Savanna	Rainforest
Latent heat	−0.17	−0.60	0.72	0.61
Sensible heat	0.04	0.32	0.25	0.54
Ground heat	0.05	0.22	0.79	0.66

Finally, we examined the effects of fires on the gross primary production (GPP) for both biomes. GPP represents the total amount of carbon fixed during photosynthesis and depends on vegetation health, and water and energy availability. Unburned GPP is higher in the rainforest than in the savanna every month as expected. GPP is larger during the wet season and reaches its lowest values at the end of the dry season in both biomes (Figure 7a). The vegetation degradation associated with fires decreases carbon sequestration in both ecoregions (Figure 7b). The largest drop occurs between September and December for both ecoregions. The GPP annual change at the savanna and rainforest areas, with at least 20% burned, are approximately −12% and −10%, respectively. In some highly burned areas (>60% burned), GPP drops by over 30% between October and November, particularly in the savannas.

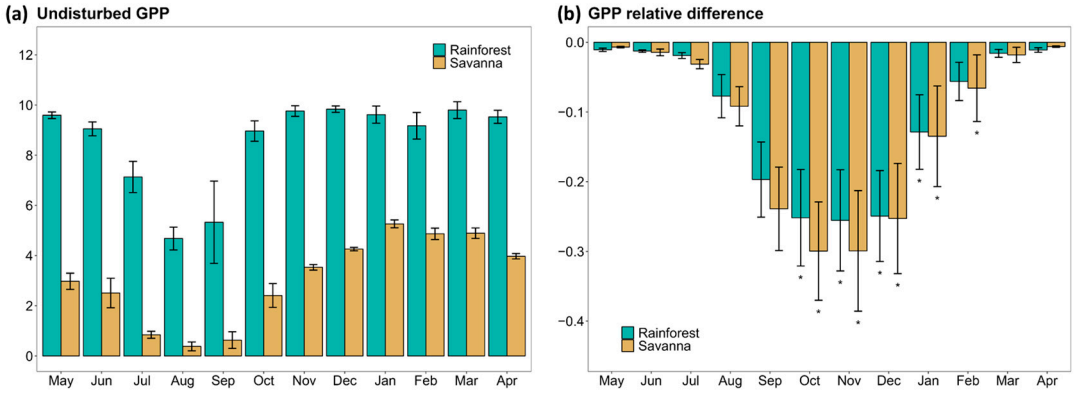

Figure 7. (**a**) Average unburned GPP (g C m^{-2} day^{-1}) and (**b**) GPP relative difference between burned and burned experiments (%) for the study area's main biomes. Error bars represent one standard deviation from the mean and asterisks in (**b**), indicating differences that are significant at a 90% confidence level. Only grid cells at least 20% burned are used for this plot.

4. Discussion

The model results discussed in the previous sessions suggest that fires have a substantial impact on the energy budget and heat partitioning at the surface in the rainforest and Cerrado regions of Brazil. Simulations indicated a decrease in evapotranspiration and atmospheric convective heating that extends well into the onset of the rainy season.

Our findings are consistent with similar studies over Northern and Southern Africa [10,11], where fire-induced vegetation and soil degradation also resulted in de-

creased precipitation rates that impacted both burned and unburned areas. The smaller burned area extent registered in the rainforest and savanna biomes of Brazil, compared to similar biomes in Africa, suggest that the fire activities would probably have a weak, if any, direct effect on precipitation in northern and central Brazil. Further studies based on fully coupled land-atmosphere model simulations or remote-sensing are needed to explore the link between fire, burned areas, and precipitation in Brazil.

Nevertheless, our results show that the effects of fires in tropical Brazil are large enough to alter the Bowen ratios between burned and unburned rainforest and savanna areas significantly. The partitioning between land latent and sensible heat fluxes plays a critical role in determining the boundary layer evolution, surface warming and hydrologic cycles, and can also be an indicator of water stress at vegetated landscapes. Whereas both unburned savanna and rainforest have similar wet-season Bowen ratios dominated by evapotranspiration (0.3 and 0.2, respectively), dry-season ratios differ substantially with the rainforest's mean value remaining low at 0.8, while the savanna ratio increases to 3.5, signaling a much warmer and drier climate.

Our simulations indicated that fires induce an increase in the average Bowen ratio in both biomes, which is more pronounced in the rainforest. Savanna experiences significant impacts only during the post-fire wet season when the Bowen ratio increases by 2.5%. Fire effects are more persistent in rainforest burned sites where the Bowen ratio increases by 11% during the fire season and 4% in the post-fire wet season. The effects of vegetation removal, albedo and Bowen-ratio changes associated with fires are also evident in the near-surface air temperature and relative humidity (Figure 8). Average air temperatures over rainforest burned points increase during most of the dry season and peak in October. On the other hand, savanna burned sites experience a weak cooling primarily between September and January (Figure 8a).

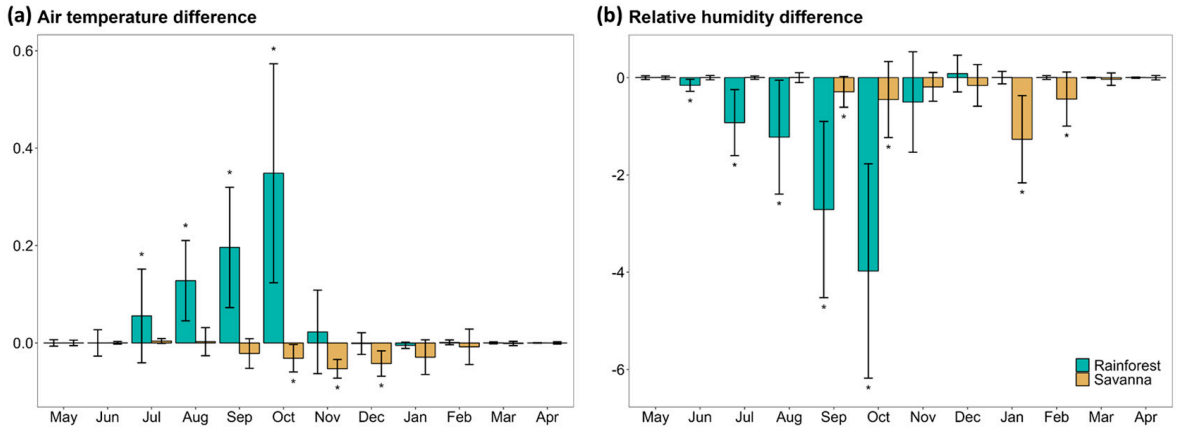

Figure 8. (**a**) Average monthly near-surface (**a**) air temperature and (**b**) relative humidity difference between burned and unburned experiments. Error bars represent one standard deviation from the mean and the asterisks in (**b**) indicate differences that are significant at a 90% confidence level. Only grid cells at least 20% burned are used for this plot.

Burned sites in both biomes experience drier conditions following fires. Rainforest humidity impacts are concentrated during the fire season, while in the savanna they happen primarily in the late fire-season and wet season (Figure 8b). Again, overall the impacts are stronger over rainforest burned areas. While the magnitude of the impacts in the air temperature and humidity may be seen as small, it should be noted that fires occur at different points at different times during the whole season so that the monthly averages may underestimate local effects over a specific burned area. Furthermore, these results do not include the effects of the land–atmosphere processes feedback. For instance, post-fire surface drying could lead to decreased convective instability that could result in reduced

cloud-cover and less precipitation in and around burned areas, further drying and warming the near-surface air [10].

Climate change is projected to increase seasonal climate variations in parts of Brazil including along the rainforest-savanna transition region [46], and there is evidence that dry-season intensification is already increasing in the southern part of the Amazon Basin. Observations indicate that the dry-season length in southern Amazonia has increased since 1979, primarily due to a delay of the rainy-season onset, which is accompanied by a prolonged fire season. These changes cannot be directly linked to the variability of the tropical Pacific and Atlantic Oceans, and further studies are needed to attribute them to anthropogenic forcing [47]. Drier conditions along the rainforest–savanna transition zone have been found to be consistent with tree mortality trends observed in forest plots established in the early 1980s [48].

While cattle intensification on current pastureland has been viewed as a potential means to avert ranchers' historic dependence on Amazon and Cerrado slash-and-burn practices [49], the increasing demand for water with a growing cattle herd could result in additional negative environmental footprints in the region under a drying dry-season climate. Coupled with the recent surges in deforestation rates in the area, linked to increasing economic pressures and recent weakening of environmental agencies and federal legislation [22], we should expect the burned area extents to increase in northern and central Brazil, leading to the intensification of the environmentally negative effects described in this study.

5. Conclusions

We used a combined approach based on remote sensing and numerical modeling to quantify the effects of burned areas on the surface climate of Brazil's biomes most affected by fires: the tropical savanna and Amazon rainforest. The results indicate that latent heat flux decreases by approximately 0.17 W m^{-2} in the savanna and 0.60 W m^{-2} in the rainforest per each 1 km^2 burned on average, with most of the impacts registered between November and December in the savanna and September and October in the rainforest. Fires also caused sensible and ground heat fluxes to increase in both biomes, however, these changes were either less significant or weaker than those simulated for evapotranspiration.

Overall, the changes in vegetated cover, surface roughness, albedo, and energy partitioning associated with fires resulted in drier and warmer near-surface conditions over rainforest burned areas, and drier but slightly cooler conditions over savanna burned areas. The impacts on air temperature and relative humidity were more pronounced in the rainforest burned areas. Fires also lowered the gross primary production in both biomes, with the largest drop occurring between September and December. Post-fire gross primary production decreased on average by 12% and 10%, in the savanna and rainforest, respectively.

Whether the amount of burned area registered in the Brazilian rainforest and savanna regions over the last decades has been sufficient to affect rainfall and have a positive feedback on the surface drying and warming needs to be further investigated. Similarly, the complex relationship between the burned area extent and sensible heat flux changes must be disentangled before the full significance of fire effects can be fully understood. Nevertheless, fire impacts on the air temperature and relative humidity discussed could reinforce the projected drying trends for the study area linked to global warming and to recent increasing deforestation, which would favor weather conditions that support longer fires and larger burned areas. Negative interactions between climate change, deforestation, and fires could thrust both Brazilian biomes to an environmental tipping point from which they may not be able to recover.

Author Contributions: Conceptualization, F.D.S. and Z.W.; methodology, F.D.S. and Z.W.; software, F.D.S. and Z.W.; validation, F.D.S. and Z.W.; formal analysis, F.D.S. and Z.W.; writing—original draft preparation, F.D.S., Z.W. and J.G.d.S.R.; writing—review and editing, F.D.S., Z.W. and J.G.d.S.R.; project administration, F.D.S.; funding acquisition, F.D.S. All authors have read and agreed to the published version of the manuscript.

Funding: This research was funded by the National Science Foundation under Grant BCS-1825046. Additional computing support was provided by the San Diego State University's Center for Earth Systems Analysis Research.

Institutional Review Board Statement: Not applicable.

Informed Consent Statement: Not applicable.

Data Availability Statement: The data sets used for this research are available at De Sales, Fernando (2020), "SA_Burned_Area" Mendeley Data, V1 (https://doi.org/10.17632/d9d9m8m5ph.1).

Conflicts of Interest: The authors declare no conflict of interest. The funding agency had no role in the design of the study; in the collection, analyses, or interpretation of data; in the writing of the manuscript; or in the decision to publish the results.

References

1. Archibald, S.; Lehmann, C.E.R.; Gómez-Dans, J.L.; Bradstock, R.A. Defining Pyromes and Global Syndromes of Fire Regimes. *Proc. Natl. Acad. Sci. USA* **2013**, *110*, 6442–6447. [CrossRef]
2. Bond, W.J.; Keeley, J.E. Fire as a Global 'Herbivore': The Ecology and Evolution of Flammable Ecosystems. *Trends Ecol. Evol.* **2005**, *20*, 387–394. [CrossRef]
3. Bowman, D.M.J.S.; Balch, J.K.; Artaxo, P.; Bond, W.J.; Carlson, J.M.; Cochrane, M.A.; D'Antonio, C.M.; DeFries, R.S.; Doyle, J.C.; Harrison, S.P.; et al. Fire in the Earth System. *Science* **2009**, *324*, 481–484. [CrossRef]
4. Bowman, D.M.J.S.; Balch, J.; Artaxo, P.; Bond, W.J.; Cochrane, M.A.; D'Antonio, C.M.; DeFries, R.; Johnston, F.H.; Keeley, J.E.; Krawchuk, M.A.; et al. The Human Dimension of Fire Regimes on Earth. *J. Biogeogr.* **2011**, *38*, 2223–2236. [CrossRef]
5. Silveira, M.V.F.; Petri, C.A.; Broggio, I.S.; Chagas, G.O.; Macul, M.S.; Leite, C.C.S.S.; Ferrari, E.M.M.; Amim, C.G.V.; Freitas, A.L.R.; Motta, A.Z.V.; et al. Drivers of Fire Anomalies in the Brazilian Amazon: Lessons Learned from the 2019 Fire Crisis. *Land* **2020**, *9*, 516. [CrossRef]
6. Rother, D.; De Sales, F. Impact of Wildfire on the Surface Energy Balance in Six California Case Studies. *Bound.-Layer Meteorol.* **2021**, *178*, 143–166. [CrossRef]
7. Whitman, E.; Parks, S.A.; Holsinger, L.M.; Parisien, M.-A. Climate-Induced Fire Regime Amplification in Alberta, Canada. *Environ. Res. Lett.* **2022**, *17*, 055003. [CrossRef]
8. Dupuy, J.; Fargeon, H.; Martin-StPaul, N.; Pimont, F.; Ruffault, J.; Guijarro, M.; Hernando, C.; Madrigal, J.; Fernandes, P. Climate Change Impact on Future Wildfire Danger and Activity in Southern Europe: A Review. *Ann. For. Sci.* **2020**, *77*, 35. [CrossRef]
9. Abram, N.J.; Henley, B.J.; Sen Gupta, A.; Lippmann, T.J.R.; Clarke, H.; Dowdy, A.J.; Sharples, J.J.; Nolan, R.H.; Zhang, T.; Wooster, M.J.; et al. Connections of Climate Change and Variability to Large and Extreme Forest Fires in Southeast Australia. *Commun. Earth Environ.* **2021**, *2*, 8. [CrossRef]
10. De Sales, F.; Xue, Y.K.; Okin, G.S. Impact of Burned Areas on the Northern African Seasonal Climate from the Perspective of Regional Modeling. *Clim. Dyn.* **2016**, *47*, 3393–3413. [CrossRef]
11. De Sales, F.; Okin, G.S.; Xue, Y.; Dintwe, K. On the Effects of Wildfires on Precipitation in Southern Africa. *Clim. Dyn.* **2019**, *52*, 951–967. [CrossRef]
12. Rother, D.E.; Sales, F.D.; Stow, D.; McFadden, J. Impacts of Burn Severity on Short-Term Postfire Vegetation Recovery, Surface Albedo, and Land Surface Temperature in California Ecoregions. *PLoS ONE* **2022**, *17*, e0274428. [CrossRef] [PubMed]
13. Boegelsack, N.; Withey, J.; O'Sullivan, G.; McMartin, D. A Critical Examination of the Relationship between Wildfires and Climate Change with Consideration of the Human Impact. *J. Environ. Prot.* **2018**, *9*, 461–467. [CrossRef]
14. Oris, F.; Asselin, H.; Ali, A.A.; Finsinger, W.; Bergeron, Y. Effect of Increased Fire Activity on Global Warming in the Boreal Forest. *Environ. Rev.* **2014**, *22*, 206–219. [CrossRef]
15. Prosperi, P.; Bloise, M.; Tubiello, F.N.; Conchedda, G.; Rossi, S.; Boschetti, L.; Salvatore, M.; Bernoux, M. New Estimates of Greenhouse Gas Emissions from Biomass Burning and Peat Fires Using MODIS Collection 6 Burned Areas. *Clim. Chang.* **2020**, *161*, 415–432. [CrossRef]
16. van der Werf, G.R.; Randerson, J.T.; Giglio, L.; van Leeuwen, T.T.; Chen, Y.; Rogers, B.M.; Mu, M.; van Marle, M.J.E.; Morton, D.C.; Collatz, G.J.; et al. Global Fire Emissions Estimates during 1997–2016. *Earth Syst. Sci. Data* **2017**, *9*, 697–720. [CrossRef]
17. Lasslop, G.; Hantson, S.; Harrison, S.P.; Bachelet, D.; Burton, C.; Forkel, M.; Forrest, M.; Li, F.; Melton, J.R.; Yue, C.; et al. Global Ecosystems and Fire: Multi-Model Assessment of Fire-Induced Tree-Cover and Carbon Storage Reduction. *Glob. Chang. Biol.* **2020**, *26*, 5027–5041. [CrossRef]
18. Tian, C.; Yue, X.; Zhu, J.; Liao, H.; Yang, Y.; Lei, Y.; Zhou, X.; Zhou, H.; Ma, Y.; Cao, Y. Fire–Climate Interactions through the Aerosol Radiative Effect in a Global Chemistry–Climate–Vegetation Model. *Atmos. Chem. Phys.* **2022**, *22*, 12353–12366. [CrossRef]
19. Zou, Y.; Wang, Y.; Qian, Y.; Tian, H.; Yang, J.; Alvarado, E. Using CESM-RESFire to Understand Climate–Fire–Ecosystem Interactions and the Implications for Decadal Climate Variability. *Atmos. Chem. Phys.* **2020**, *20*, 995–1020. [CrossRef]
20. Pivello, V.R. The Use of Fire in the Cerrado and Amazonian Rainforests of Brazil: Past and Present. *Fire Ecol.* **2011**, *7*, 24–39. [CrossRef]

21. Gatti, L.V.; Basso, L.S.; Miller, J.B.; Gloor, M.; Gatti Domingues, L.; Cassol, H.L.G.; Tejada, G.; Aragão, L.E.O.C.; Nobre, C.; Peters, W.; et al. Amazonia as a Carbon Source Linked to Deforestation and Climate Change. *Nature* **2021**, *595*, 388–393. [CrossRef]
22. De Sales, F.; Santiago, T.; Biggs, T.W.; Mullan, K.; Sills, E.O.; Monteverde, C. Impacts of Protected Area Deforestation on Dry-Season Regional Climate in the Brazilian Amazon. *J. Geophys. Res. Atmos.* **2020**, *125*, e2020JD033048. [CrossRef]
23. Pellegrini, A.F.A.; Anderegg, W.R.L.; Paine, C.E.T.; Hoffmann, W.A.; Kartzinel, T.; Rabin, S.S.; Sheil, D.; Franco, A.C.; Pacala, S.W. Convergence of Bark Investment According to Fire and Climate Structures Ecosystem Vulnerability to Future Change. *Ecol. Lett.* **2017**, *20*, 307–316. [CrossRef]
24. Pereira, A.A.; Pereira, J.M.C.; Libonati, R.; Oom, D.; Setzer, A.W.; Morelli, F.; Machado-Silva, F.; De Carvalho, L.M.T. Burned Area Mapping in the Brazilian Savanna Using a One-Class Support Vector Machine Trained by Active Fires. *Remote Sens.* **2017**, *9*, 1161. [CrossRef]
25. Giglio, L.; Boschetti, L.; Roy, D.P.; Humber, M.L.; Justice, C.O. The Collection 6 MODIS Burned Area Mapping Algorithm and Product. *Remote Sens. Environ.* **2018**, *217*, 72–85. [CrossRef]
26. Cochrane, M.A.; Alencar, A.; Schulze, M.D.; Souza, C.M.; Nepstad, D.C.; Lefebvre, P.; Davidson, E.A. Positive Feedbacks in the Fire Dynamic of Closed Canopy Tropical Forests. *Science* **1999**, *284*, 1832–1835. [CrossRef]
27. Nepstad, D.; Carvalho, G.; Cristina Barros, A.; Alencar, A.; Paulo Capobianco, J.; Bishop, J.; Moutinho, P.; Lefebvre, P.; Lopes Silva, U.; Prins, E. Road Paving, Fire Regime Feedbacks, and the Future of Amazon Forests. *For. Ecol. Manag.* **2001**, *154*, 395–407. [CrossRef]
28. Ramos-Neto, M.B.; Pivello, V.R. Lightning Fires in a Brazilian Savanna National Park: Rethinking Management Strategies. *Environ. Manag.* **2000**, *26*, 675–684. [CrossRef]
29. Zhan, X.W.; Xue, Y.K.; Collatz, G.J. An Analytical Approach for Estimating CO2 and Heat Fluxes over the Amazonian Region. *Ecol. Model.* **2003**, *162*, 97–117. [CrossRef]
30. Hersbach, H.; Bell, B.; Berrisford, P.; Hirahara, S.; Horányi, A.; Muñoz-Sabater, J.; Nicolas, J.; Peubey, C.; Radu, R.; Schepers, D.; et al. The ERA5 Global Reanalysis. *Q. J. R. Meteorol. Soc.* **2020**, *146*, 1999–2049. [CrossRef]
31. Xu, M.; Zhang, X.; Liang, X.Z. *MODIS-Derived Vegetation and Albedo Parameters for Agroecosystem-Climate Modeling*; ORNL DAAC: Oak Ridge, TN, USA, 2018. [CrossRef]
32. Lyons, E.; Jin, Y.; Randerson, J. Changes in Surface Albedo after Fire in Boreal Forest Ecosystems of Interior Alaska Assessed Using MODIS Satellite Observations. *J. Geophys. Res.-Biogeosci.* **2008**, *113*. [CrossRef]
33. Huang, H.; Xue, Y.; Liu, Y.; Li, F.; Okin, G.S. Modeling the Short-Term Fire Effects on Vegetation Dynamics and Surface Energy in Southern Africa Using the Improved SSiB4/TRIFFID-Fire Model. *Geosci. Model Dev.* **2021**, *14*, 7639–7657. [CrossRef]
34. Gatebe, C.K.; Ichoku, C.M.; Poudyal, R.; Roman, M.O.; Wilcox, E. Surface Albedo Darkening from Wildfires in Northern Sub-Saharan Africa. *Environ. Res. Lett.* **2014**, *9*, 065003. [CrossRef]
35. Simon, M.F.; Pennington, T. Evidence for adaptation to fire regimes in the tropical savannas of the Brazilian Cerrado. *Int. J. Plant Sci.* **2012**, *173*, 711–723. [CrossRef]
36. Dintwe, K.; Okin, G.S.; Xue, Y.K. Fire-Induced Albedo Change and Surface Radiative Forcing in Sub-Saharan Africa Savanna Ecosystems: Implications for the Energy Balance. *J. Geophys. Res.-Atmos.* **2017**, *122*, 6186–6201. [CrossRef]
37. Jin, Y.; Randerson, J.T.; Goetz, S.J.; Beck, P.S.A.; Loranty, M.M.; Goulden, M.L. The Influence of Burn Severity on Postfire Vegetation Recovery and Albedo Change during Early Succession in North American Boreal Forests. *J. Geophys. Res. Biogeosci.* **2012**, *117*. [CrossRef]
38. Didan, K.; Munoz, A.B.; Huete, A. MODIS Vegetation Index User's Guide (MOD13 Series) Version 3.00 2015. Vegetation Index and Phenology Lab, University of Arizona: Tucson, AZ, USA, 2015.
39. Schaaf, C.; Wang, Z. *MCD43A1 MODIS/Terra + Aqua BRDF/Albedo Model Parameters Daily L3 Global—500m V006*; NASA EOSDIS Land Processes DAAC: Sioux Falls, SD, USA, 2015.
40. Rodell, M.; Houser, P.R.; Jambor, U.; Gottschalck, J.; Mitchell, K.; Meng, C.-J.; Arsenault, K.; Cosgrove, B.; Radakovich, J.; Bosilovich, M.; et al. The Global Land Data Assimilation System. *Bull. Am. Meteorol. Soc.* **2004**, *85*, 381–394. [CrossRef]
41. Legates, D.R.; Willmott, C.J. Mean Seasonal and Spatial Variability in Gauge-Corrected, Global Precipitation. *Int. J. Climatol.* **1990**, *10*, 111–127. [CrossRef]
42. Harris, I.; Jones, P.D.; Osborn, T.J.; Lister, D.H. Updated High-Resolution Grids of Monthly Climatic Observations—The CRU TS3.10 Dataset. *Int. J. Climatol.* **2014**, *34*, 623–642. [CrossRef]
43. Lawrimore, J.H.; Menne, M.J.; Gleason, B.E.; Williams, C.N.; Wuertz, D.B.; Vose, R.S.; Rennie, J. An Overview of the Global Historical Climatology Network Monthly Mean Temperature Data Set, Version 3. *J. Geophys. Res. Atmos.* **2011**, *116*. [CrossRef]
44. Fan, Y.; van den Dool, H. A Global Monthly Land Surface Air Temperature Analysis for 1948–Present. *J. Geophys. Res. Atmos.* **2008**, *113*. [CrossRef]
45. Koenker, R.; Bassett, G. Regression Quantiles. *Econometrica* **1978**, *46*, 33–50. [CrossRef]
46. Boisier, J.P.; Ciais, P.; Ducharne, A.; Guimberteau, M. Projected Strengthening of Amazonian Dry Season by Constrained Climate Model Simulations. *Nat. Clim. Chang.* **2015**, *5*, 656. [CrossRef]
47. Fu, R.; Yin, L.; Li, W.; Arias, P.A.; Dickinson, R.E.; Huang, L.; Chakraborty, S.; Fernandes, K.; Liebmann, B.; Fisher, R.; et al. Increased Dry-Season Length over Southern Amazonia in Recent Decades and Its Implication for Future Climate Projection. *Proc. Natl. Acad. Sci. USA* **2013**, *110*, 18110–18115. [CrossRef] [PubMed]

48. Gloor, M.; Barichivich, J.; Ziv, G.; Brienen, R.; Schöngart, J.; Peylin, P.; Ladvocat Cintra, B.B.; Feldpausch, T.; Phillips, O.; Baker, J. Recent Amazon Climate as Background for Possible Ongoing and Future Changes of Amazon Humid Forests. *Glob. Biogeochem. Cycles* **2015**, *29*, 1384–1399. [CrossRef]
49. Lathuillière, M.J.; Solvik, K.; Macedo, M.N.; Graesser, J.; Miranda, E.J.; Couto, E.G.; Johnson, M.S. Cattle Production in Southern Amazonia: Implications for Land and Water Management. *Environ. Res. Lett.* **2019**, *14*, 114025. [CrossRef]